

# A Triple-Band CMOS Power Amplifier Using Multi-Band and Switchable Matching Network for Wireless Mobile

Milim Lee, *Student Member, IEEE*, and Changkun Park<sup>✉</sup>, *Member, IEEE*

**Abstract**—A triple-band CMOS power amplifier (PA) is presented. We propose a design methodology using an input matching network to support triple-band operation at 0.9, 1.8, and 2.4 GHz. We also propose an output matching network for the triple-band operation. Given that 1.8 and 2.4 GHz are the harmonic components when the PA is operating at 0.9 GHz, we design the output matching network to be switchable to suppress the harmonic components at the operating frequency. Using this switchable network, we obtain an optimum power matching point for each of the three operating frequencies. To verify the feasibility of the proposed structure, we designed a PA using a 180-nm RFCMOS process. It was measured using a wideband code division multiple access (WCDMA), Long-Term Evolution (LTE) at a 10/20-MHz bandwidth and wireless local area network (WLAN) 802.11n applications. The measured output power was 27.2/26.6 dBm, and the power-added efficiency (PAE) was 22.9%/30.6% under an adjacent channel leakage ratio (ACLR) of -33 dBc at 0.9/1.8 GHz, respectively, with a WCDMA modulation signal. In the case of an LTE modulation signal, the measured output power was 25.1/23.5 dBm, and the PAE was 27.7%/23.6% under an ACLR of -30 dBc for a 10/20-MHz bandwidth, respectively, at 1.8 GHz. The measured output power was 21 dBm, and the PAE was 20% under an error vector magnitude (EVM) of 3.98% at 2.4 GHz for a WLAN modulation signal. Based on the measured results, we successfully verified the feasibility of the proposed PA.

**Index Terms**—CMOS, Long-Term Evolution (LTE), matching network, power amplifiers (PAs), transformer, triple-band, wideband code division multiple access (WCDMA), wireless local area network (WLAN).

## I. INTRODUCTION

WITH the rapid growth rate of modern wireless mobile devices, the generation of mobile data is also rapidly increasing. Therefore, modern wireless mobile communication (3G/4G) requires more sophisticated technology than existing mobile communication (2G). Moreover, apart from the technological advancement required to facilitate new

Manuscript received November 25, 2018; revised February 26, 2019 and April 21, 2019; accepted June 25, 2019. Date of publication August 15, 2019; date of current version October 4, 2019. This work was supported by the Korean Ministry of Trade, Industry and Energy through the Industrial Strategic Technology Development Program under Grant 10053023. (*Corresponding author: Changkun Park*)

The authors are with the School of Electronic Engineering, College of Information Technology, Soongsil University, Seoul 06978, South Korea (e-mail: mlgirlm@ssu.ac.kr; pck77@ssu.ac.kr).

Color versions of one or more of the figures in this article are available online at <http://ieeexplore.ieee.org>.

Digital Object Identifier 10.1109/TMTT.2019.2931899

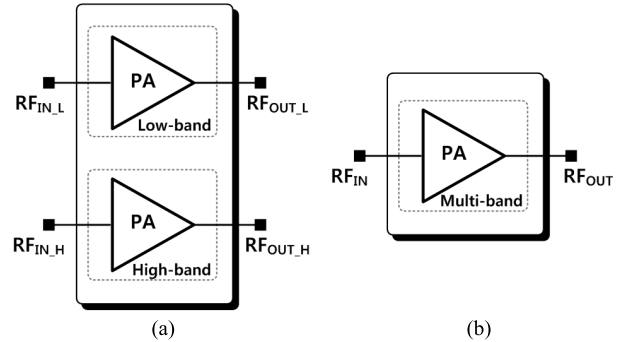


Fig. 1. Block diagram of PA. (a) Multi-PA and (b) single-PA solution for multiband applications.

wireless communication, the continued application of existing communication standards is also necessary. That is, 2G protocols [such as global system for mobile communications (GSM)] are still in “continuous” demand for wireless communication, along with 3G protocols [such as wideband code division multiple access (WCDMA)], and 4G protocols [such as Long-Term Evolution (LTE)], wireless local area network (WLAN), etc. Accordingly, a technology capable of satisfying all communication standards in one device is required [1]–[8]. RF systems require multichip power amplifiers (PAs), such as high-band PAs and low-band PAs to meet the linearity requirements of 3G, 4G, and WLAN protocols in a single mobile device, as shown in Fig. 1(a) [9]–[13]. In particular, the PA occupies a large area in the device, which leads to increased cost in the case of a multichip approach for multiband support. In addition, the switches and control logic for control of the operation of the PA is required for each wireless communication. Therefore, multiband support using a single PA, as shown in Fig. 1(b) is required.

Accordingly, several techniques have been reported to support multiband based on a single PA [14]–[17]. However, most of the multiband PAs are designed to support dual-band applications. For example, the previously studied quad-band PA supports 0.8/0.9 and 1.8/1.9 GHz. Accordingly, the PA is effectively a dual-band PA [9]. There is a need for research on triple-band PAs to support additional standards. Various techniques that have been adapted to the dual-band PA could be used in the triple-band PA to design a triple-band PA. However, if the techniques are adapted to the triple-band PA,

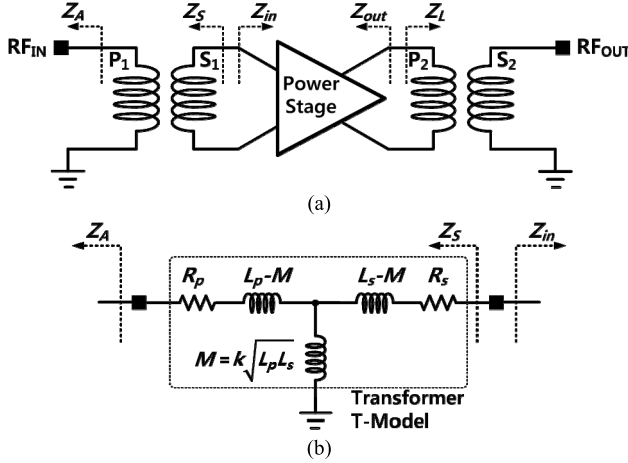


Fig. 2. (a) Single-stage CMOS PA. (b) Input transformer of the input matching network T-model equivalent circuit.

several switches are required to select each frequency band. In this case, some problems related to the degradation of output power and efficiency could arise.

In this work, we design a single PA to support the triple bands of 0.9, 1.8, and 2.4 GHz. In order to minimize performance degradation, we propose a design methodology for a multiband input matching network without using additional circuits or switches. We also propose a design for the structure of the output matching network based on the load-pull simulation to support triple band. In addition, we solve the problems associated with the harmonic components of the 0.9-GHz operating frequency via the proposed output matching network.

## II. PROPOSED INPUT MATCHING NETWORK

### A. Design of Wideband Transformer

We design a triple-band PA with a differential and cascode structure to address the problems associated with CMOS based RF circuits [18]. In this work, a transformer is used as the input balun as well as the input matching component. Although most of the previous works related to the PA are focused on the optimization of the output matching network [18]–[20], the loss induced by the input matching network should also be minimized to obtain sufficient gain for each frequency band of the triple-band PA.

Fig. 2(a) shows the location of the input matching network, including the input transformer. Fig. 2(b) shows the details of the input matching network component, and the transformer is represented by the easy-to-interpret T-model [21], [22]. The impedance of the source is represented by Z<sub>A</sub>, and generally, 50 Ω is used. First, we determine Z<sub>in</sub> to construct the triple-band input matching network. This value is determined by the power-cell of the power stage, the design of which is described in Section III-B. As shown in Fig. 3, when the load impedance is 50 Ω, the values of Z<sub>in</sub> are 26.8 – j84.0, 10.7 – j42.4, and 7.4 – j28.5 Ω at 0.9, 1.8, and 2.4 GHz, respectively.

We then define the size of the input transformer. In order to simultaneously satisfy the supported frequency bands,

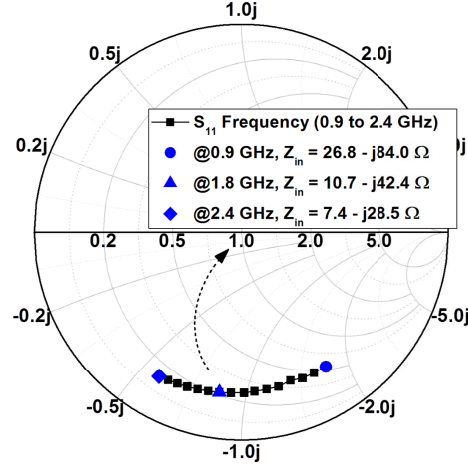


Fig. 3. Simulated S<sub>11</sub> and Z<sub>in</sub> at 0.9, 1.8, and 2.4 GHz in the input matching network.

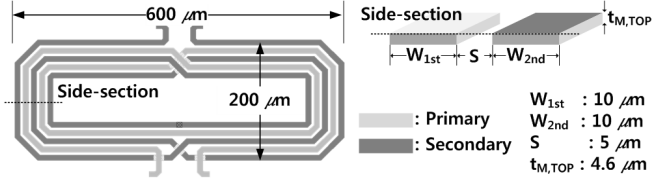


Fig. 4. Input transformer structure and parameters.

a structure with a wide bandwidth characteristic is required. The bandwidth is related to the quality factor (Q-factor) and is defined as follows for the transformer:

$$\text{Bandwidth(BW)} = \frac{\omega}{Q} \quad (1)$$

where  $\omega$  is the resonant frequency and  $Q$  is the Q-factor.

The Q-factor  $Q_p$  and  $Q_s$  of the primary and secondary windings, respectively, are expressed as

$$Q_p = \frac{\omega L_p}{R_p} \quad Q_s = \frac{\omega L_s}{R_s} \quad (2)$$

$$\text{BW} \propto R_p, R_s \quad (3)$$

where  $R_p$  and  $R_s$  are the real parts of the primary and secondary, respectively.  $L_p$  and  $L_s$  are the inductances of the primary and secondary, respectively. In order to have a transformer with a wide characteristic based on (1) and (2), then  $R_p$ ,  $R_s$ , i.e., the real part components of the impedance, must be increased.

The characteristics of the input transformer were designed based on electromagnetic (EM) simulation, and a top metal layer with a thickness of 4.6 μm was used. The metal width is 10 μm, the metal spacing between the primary and the secondary is 5 μm, and the overall transformer size was 0.6 mm × 0.2 mm, as shown in Fig. 4.

Fig. 5(a) shows the real part of the impedance for the primary and secondary windings according to the number of turns of the transformer [23], and Fig. 5(b) shows the Q-factor. As the number of turns increases, the real part of the impedance increases, and the Q-factor decreases. However, the 1: 1 turn ratio transformer also has a low Q-factor because

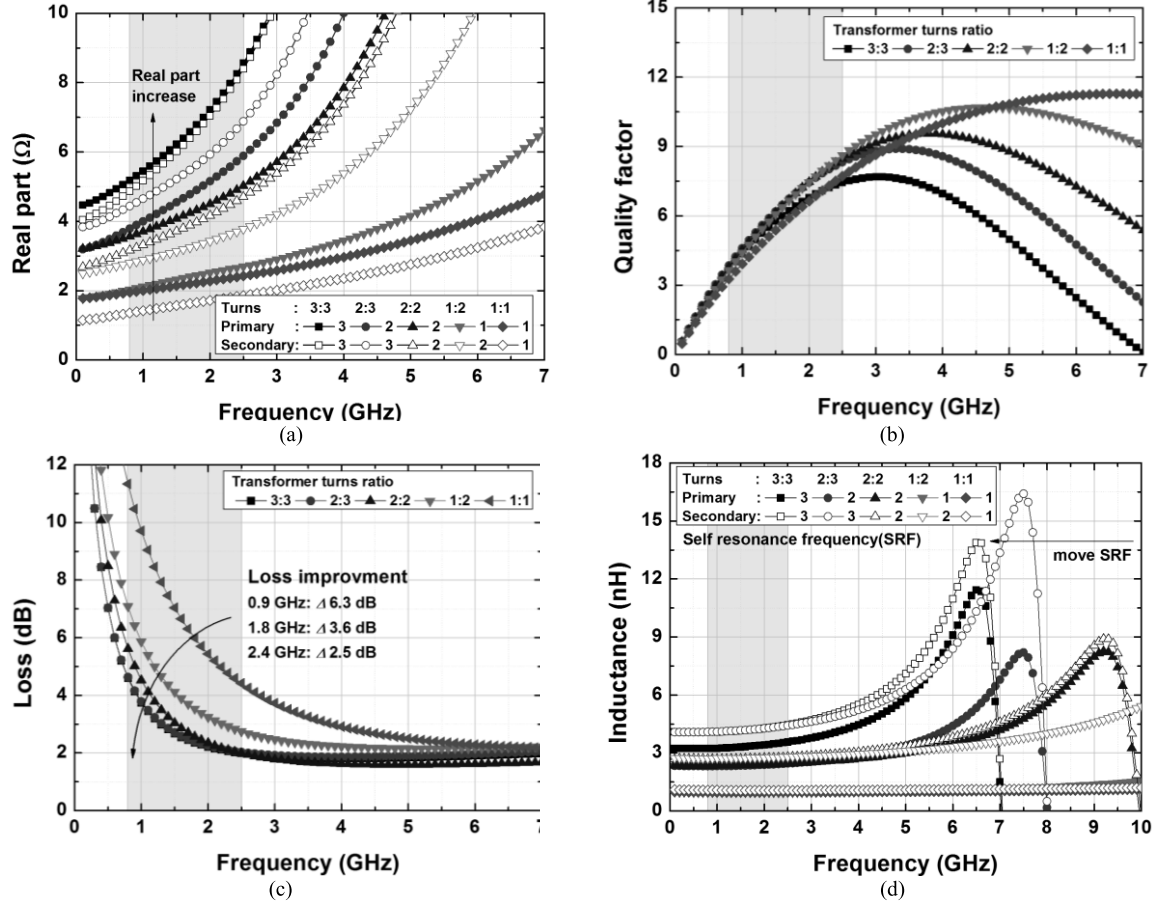


Fig. 5. Simulated results of (a) real part of the transformer impedance, (b)  $Q$ -factor, (c) loss, and (d) inductance (from 0.1 to 7.0 GHz).

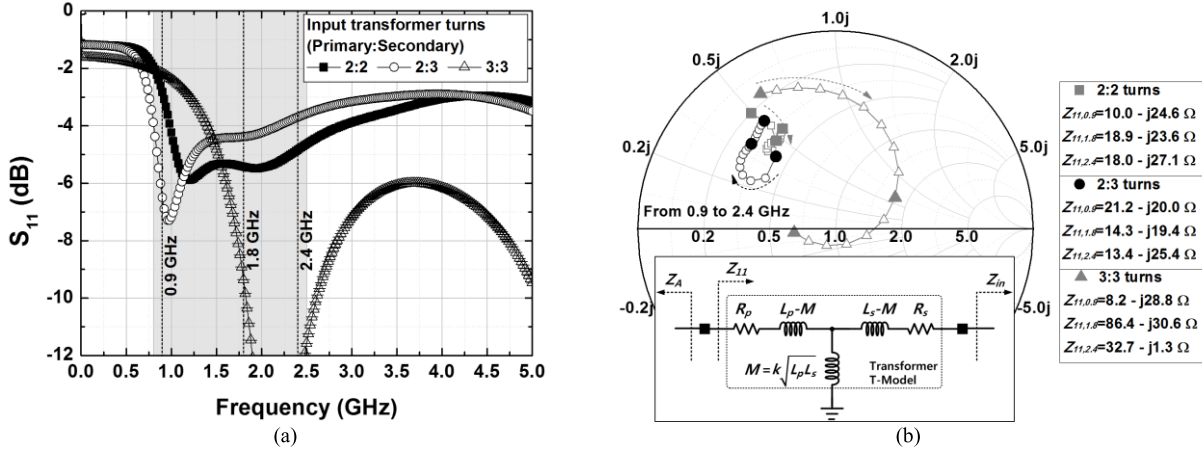


Fig. 6. Simulation results of turn analysis of the transformer. (a) Rectangular results. (b) Smith chart results.

the imaginary part, as well as the real part, has low value. Moreover, since the length where the primary and secondary windings face each other is relatively short, the magnetic coupling between the windings is weak, thereby degrading the maximum available gain (MAG). As shown in Fig. 5(c), the high loss by the transformer can lead to performance degradation. The loss in the transformer is based on the calculation of the MAG and is related to the efficiency of the

transformer [22], [24]. That is, as the number of transformer turns increases, the real part of the impedance can be increased to achieve wide bandwidth. Simultaneously, the transformer is adapted to low-band support, thereby minimizing the loss in the 0.9-GHz band. In this article, the transformers with 2:2, 2:3, and 3:3 turns ratio are considered for the support of the 0.9-, 1.8-, and 2.4-GHz bands, and the results are shown in Fig. 6. The result for  $S_{11}$ , which is an input

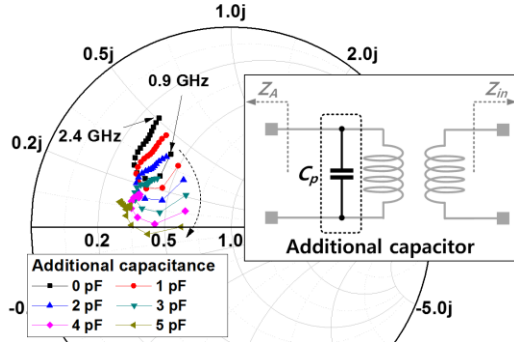


Fig. 7. Simulation results of normalized input matching network impedance with an additional parallel capacitor in the primary part (from 0.9 to 2.4 GHz).

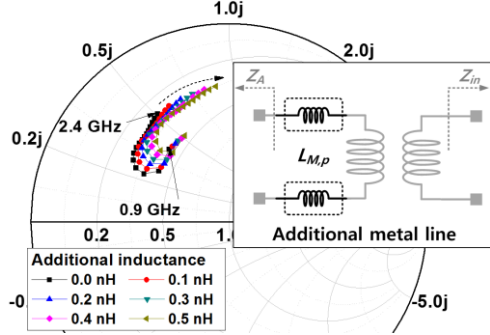


Fig. 8. Simulation results of normalized input matching network impedance with an additional series inductor in the primary part (from 0.9 to 2.4 GHz).

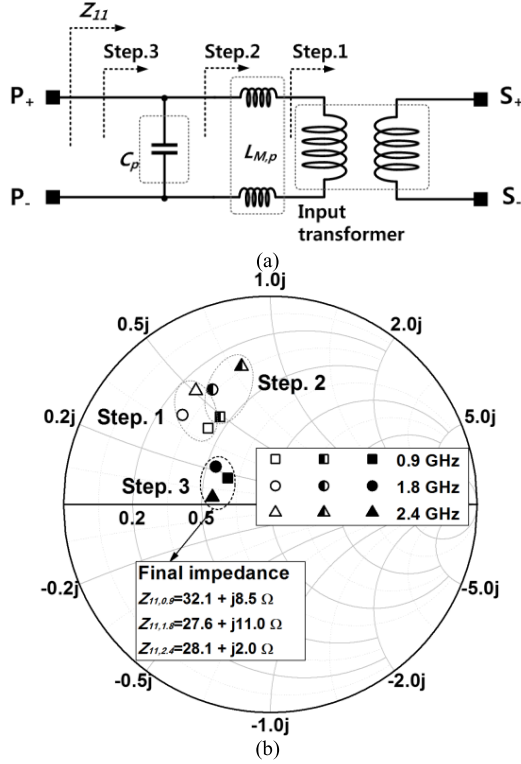


Fig. 9. (a) Proposed triple-band input matching network and (b) simulation results of normalized input matching network impedance at 0.9, 1.8, and 2.4 GHz.

matching parameter, is shown in rectangular and Smith charts for frequencies from 0.9 to 2.4 GHz. It is best to have a low-value voltage-standing wave ratio (VSWR) and to set the resistance to  $50 \Omega$  to satisfy the input impedance. Therefore,

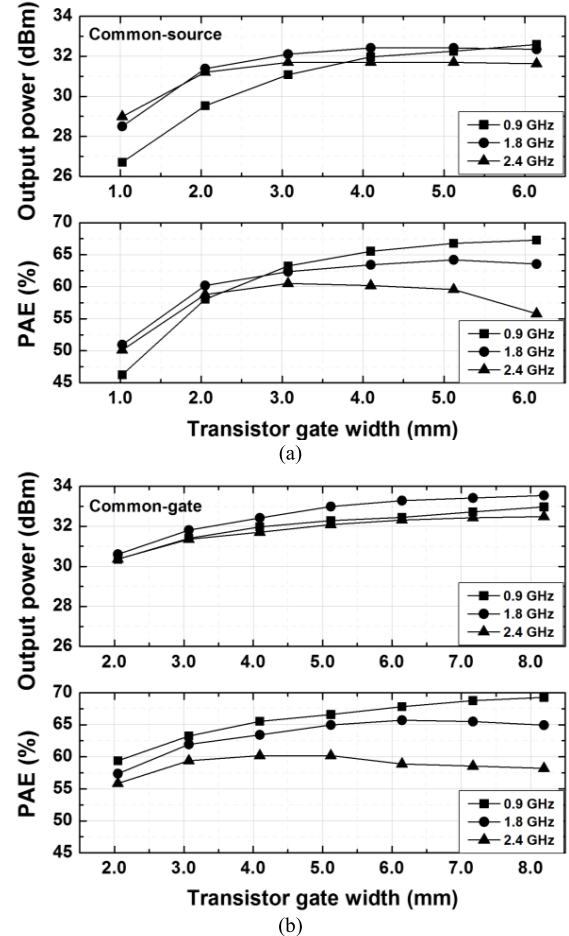


Fig. 10. Simulation results of output power and PAE of differential cascode structure at 0.9, 1.8, and 2.4 GHz at 20-dBm input power. (a) Common-source transistor power cells (gate width of common gate = 4 mm). (b) common-gate transistor power cells (gate width of common source = 4 mm).

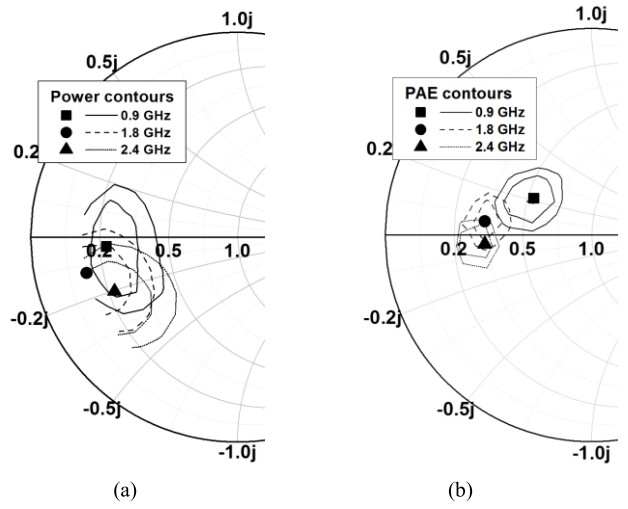


Fig. 11. Simulated load-pull maximum. (a) Output power contours and (b) PAE contours at 0.9, 1.8, and 2.4 GHz.

when the difference between the impedance values of each frequency is small, it is easy to match them simultaneously using a passive device.

The simulated  $Z_{11}$  values of the 2:3 turn ratio are  $21.8 + j23.0 \Omega$ ,  $16.0 + j17.5 \Omega$ , and  $13.3 + j20.5 \Omega$  at 0.9, 1.8,

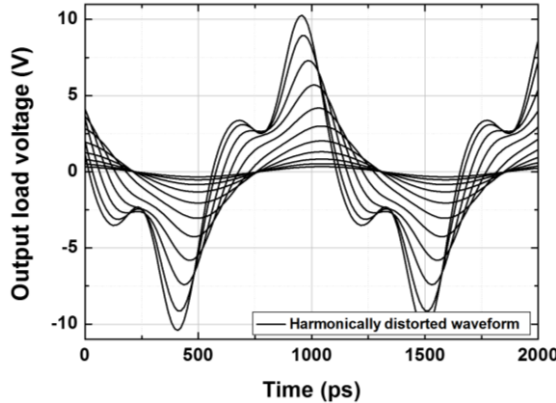


Fig. 12. Simulation results of triple-band PA output load voltage waveform at 0.9 GHz (0.9, 1.8, and 2.4 GHz have gain).

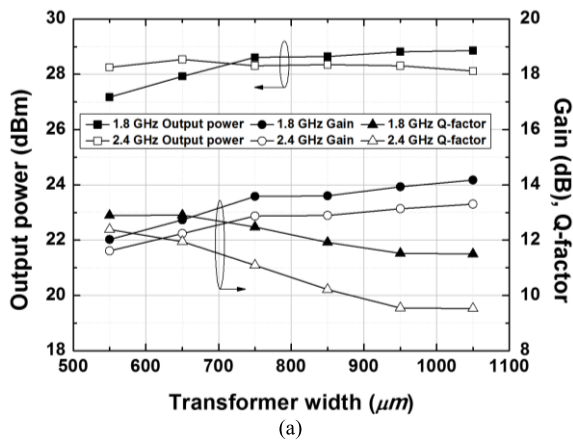


Fig. 13. (a) Simulation results of output power and gain at 1.8 and 2.4 GHz. (b) Output transformer structure and parameters.

and 2.4 GHz, respectively. Selecting 3:3 makes it more difficult to achieve simultaneous matching because an additional real part of the impedance value for 0.9 GHz is required compared to the case of 2:3. As a result, an input matching network is designed using a 2:3 turn ratio structure that is easy to match simultaneously, and the impedance conversion for 1.8 and 2.4 GHz is performed using additional components.

#### B. Components of Input Matching Network

For converting the previously obtained impedance to  $50 \Omega$ , the real component should be increased while reducing the

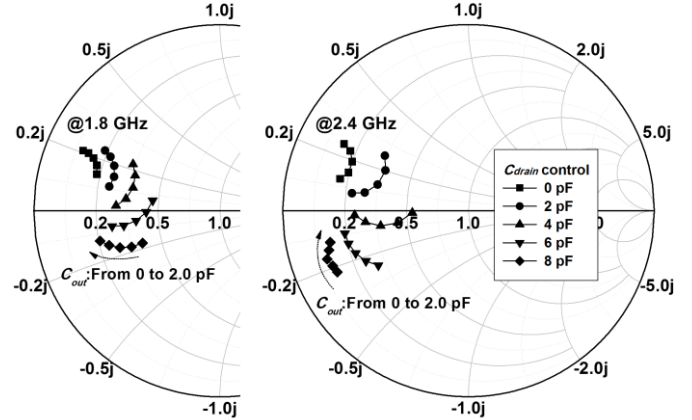


Fig. 14. Simulation results of impedance by varying the drain capacitance (from 0 to 8 pF, with steps of 2 pF) and out capacitance (from 0 to 2 pF, with steps of 0.5 pF) at 1.8 and 2.4 GHz.

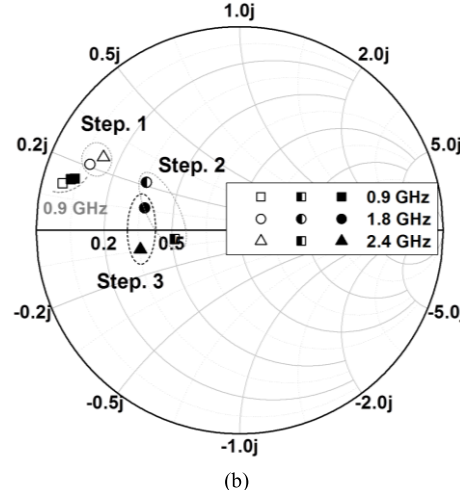
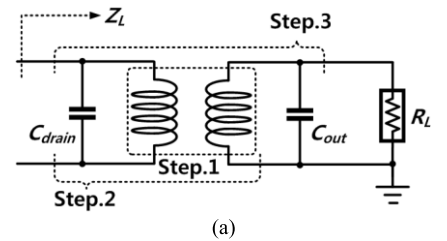


Fig. 15. (a) Final output matching network and (b) simulation results of the impedance point of the design step in the Smith chart.

imaginary component. First, an easy way to reduce the imaginary part of the impedance to zero is to use a parallel capacitor, as shown in Fig. 7. The input impedance is calculated by varying  $C_p$  when it is varied from 0 to 5 pF. When using a  $C_p$ , the impedance of the imaginary part is reduced to nearly zero. Second, it is possible to add a metal line to increase the real part of the impedance, as shown in Fig. 8. The input impedance is calculated by varying  $L_{M,p}$  from 0 to 0.5 nH. The input matching network for a triple-band is shown in Fig. 9(a), and Fig. 9(b) shows the simulation results of the scattering-parameter (S-parameter) of the input matching network impedance.

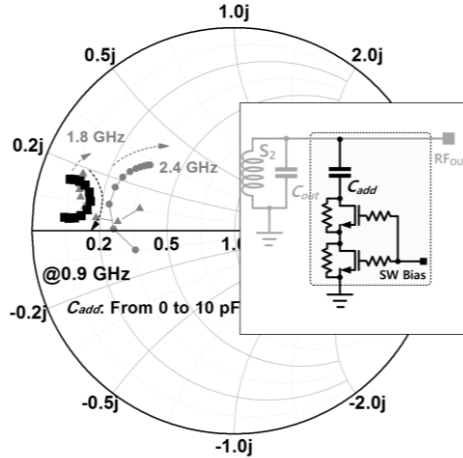


Fig. 16. Simulation results of the impedance by varying additional capacitance (from 0 to 10 pF, with steps of 1 pF) at 0.9 GHz.

In summary, the transformer structure with a wide bandwidth characteristic is initially designed to include the supported frequencies. Then the inductance and capacitance values for 50- $\Omega$  matching are used according to the characteristics of the passive device. This design methodology shows that the targeted matching impedances are well-maintained for the triple-band input matching network, simultaneously.

### III. TRIPLE-BAND PA USING SWITCHABLE OUTPUT MATCHING NETWORK

#### A. Analysis of Power-Cell Transistor

The proposed triple-band PA should be designed to provide simultaneous support using one amplification stage. Thus, we investigated the size of the transistor for maximum output power and power-added efficiency (PAE) for each frequency using load-pull simulations [25]. Fig. 10 shows the output power and PAE result with the variation of the total gate width of the common-source and common-gate transistors. For achieving an output power of 30 dBm for 10 dB gain at each frequency with one power cell structure, the total gate width size of the power cell must be defined for each frequency. In addition, the lower supply voltage of the aforementioned CMOS process results in a decrease in the load impedance with an increase of the power-cell size, which makes it difficult to design an output matching network. As a result, considering the desired output power and load impedance, a total gate width of 3.8 mm for a common-source transistor with a gate length of 180 nm and a 4.6-mm gate width for a common-gate transistor with a gate length of 350 nm are chosen for the triple-band PA, respectively.

#### B. Harmonic Issues in Triple-Band Output Matching Network

For a PA that satisfies the requirements of the triple band, impedance conversion is required such that the signal amplified through one core has the maximum performance in each frequency band. Fig. 11 shows the load-pull simulation results for 0.9, 1.8, and 2.4 GHz. In order to obtain the maximum

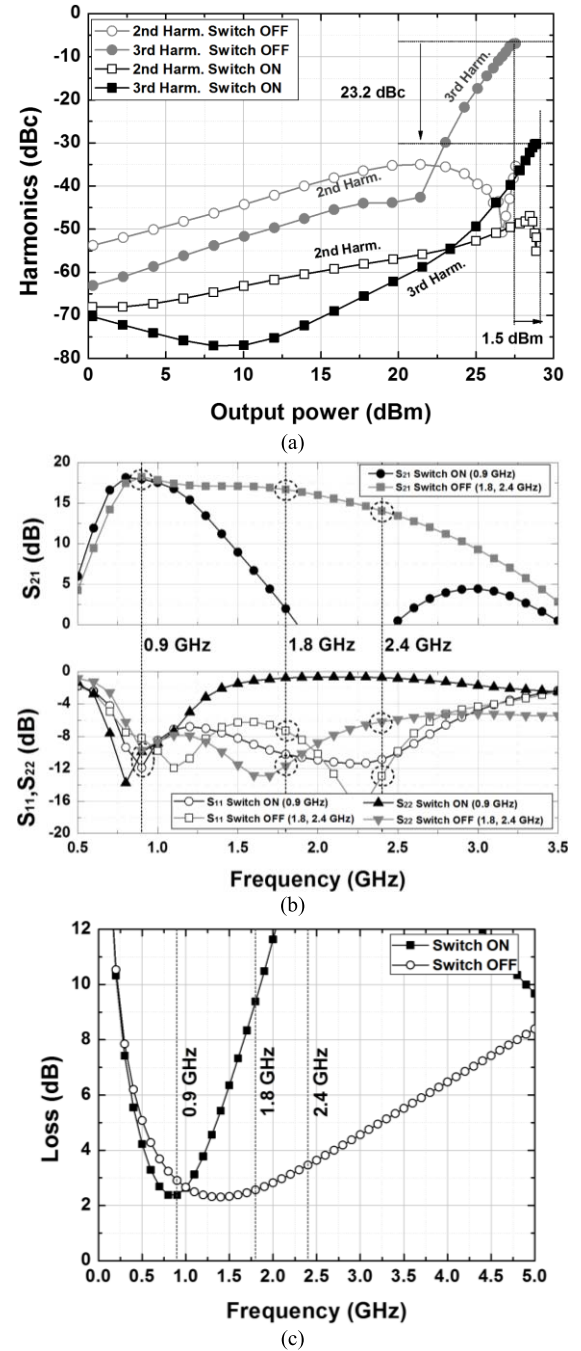


Fig. 17. Simulation results of (a) difference between the fundamental and second-harmonic switch ON and OFF at 0.9 GHz, (b) gain and  $S_{22}$ , and (c) loss.

output power and efficiency for each frequency, the impedance at each frequency must be simultaneously shifted to the respective optimum points. For achieving this, the output matching network design of the triple-band PA uses a structure that can be supported as a variable in the proposed input matching circuit to minimize the loss. It should be noted that the frequencies of the support bands should not influence each other. This is because when the input signal ( $x(t) = \cos \omega t$ ) is amplified using a transistor with nonlinearity characteristics, the output signal ( $y(t)$ ) due to harmonic distortion appears as

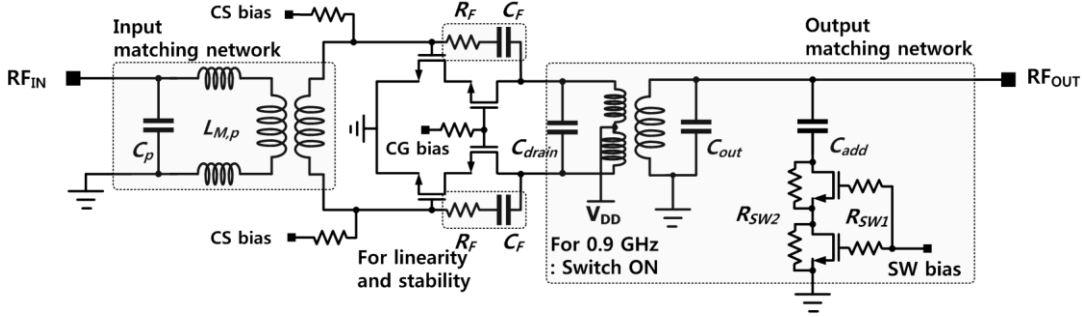


Fig. 18. Overall schematic of the CMOS triple-band PA.

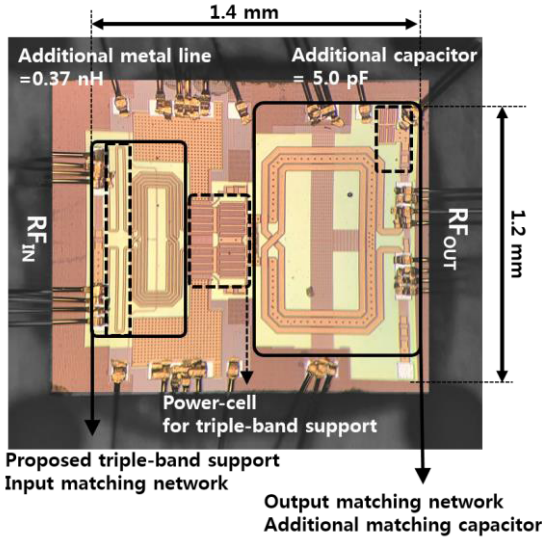


Fig. 19. Chip photograph of the triple-band PA.

follows:

$$y(t) = \frac{\alpha_1 A^2}{2} + \left( \alpha_1 A + \frac{3\alpha_3 A^3}{4} \right) \cos \omega t + \frac{\alpha_2 A^2}{2} \cos 2\omega t + \frac{\alpha_3 A^3}{2} \cos 3\omega t. \quad (4)$$

The third term is a second-harmonic, and the fourth term is a third-harmonic. If each frequency of the triple band has a similar gain at the same time, the output is simultaneously amplified to the second- and third-harmonics, as well as the fundamental, according to (4). This results in performance degradation due to the additional harmonics during fundamental frequency operation. Even compound semiconductors with better linearity than CMOS have been studied using harmonic traps and filters to address this problem [26]–[28]. Fig. 12 shows a graph of the load voltage waveform distortion due to spurious signals when a PA with a wide gain from 0.9 to 2.4 GHz operates in the 0.9-GHz band. Therefore, to solve this problem, the gain of the harmonic frequency should be suppressed when operating at 0.9 GHz. In particular, due to the characteristics of the differential structure used in CMOS PAs, gain attenuation due to third intercept point (IP3) occurs compared to second intercept point (IP2). This problem is typical in circuit design with wide characteristics at

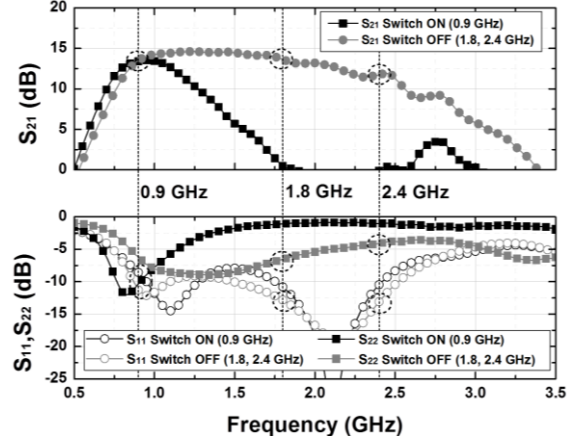


Fig. 20. Measured S-parameters (from 0.5 to 3.5 GHz).

sub-gigahertz

$$\text{Fractional Bandwidth} = \frac{2(f_H - f_L)}{f_H + f_L}. \quad (5)$$

The fractional bandwidth is a parameter that represents the characteristics of a wideband and can be expressed as (5). In this case,  $f_H$  is the maximum frequency of the 3-dB bandwidth, and  $f_L$  is the minimum frequency. If  $f_H$  is the third harmonic of  $f_L$ ,  $f_H$  becomes  $3 \times f_L$ , and the fractional bandwidth is 1. If the fractional bandwidth of a circuit is 1, it is necessary to consider the problem caused by the third harmonic.

Therefore, in order to improve the performance of the triple-band PA, 1.8 and 2.4 GHz signals are simultaneously supported without any additional circuit, and a switchable triple-band PA structure for 0.9 GHz is required.

### C. Design of Output Matching Network

As indicated in Section III-B, a switchable architecture for 0.9 GHz is required for the proposed triple-band PA design. Therefore, an output matching network that supports 1.8 and 2.4 GHz is designed, and 0.9 GHz is converted into the impedance value of the load-pull result based on the switchable technique. The results of the load-pull for each frequency are shown in Fig. 11.

First, there are some practical issues with regard to the design of the output transformer. Since the transformers used

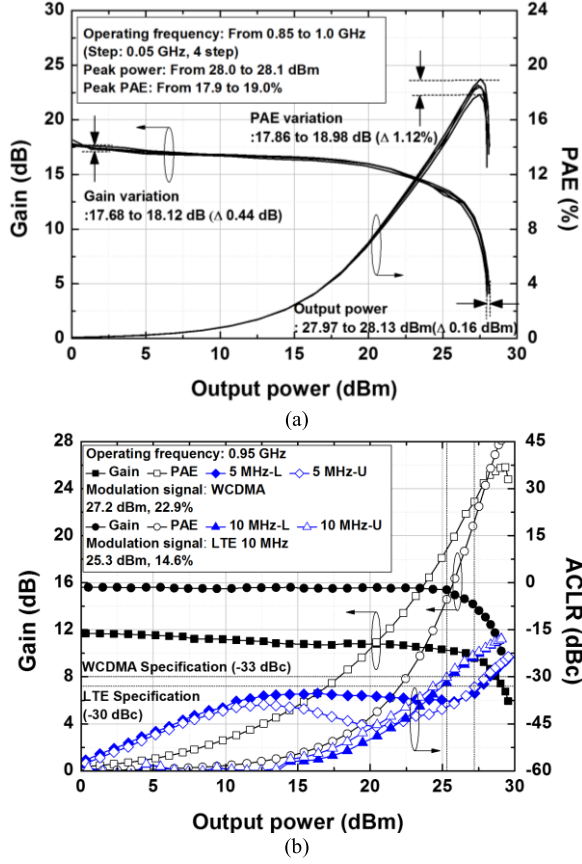


Fig. 21. (a) Measured gain, PAE, and output power of the triple-band PA for a CW signal. (b) Measured gain, PAE, ACLR, and output power of the triple-band PA for WCDMA and LTE 10-MHz signals at 0.95 GHz.

in the output matching network handles relatively large currents (several hundred milliamperes) compared to the input, a wider width compared to the input transformer is advantageous. In PAs, 1:1 or 1:2 turn ratio transformers are used to achieve a high Q-factor. In this work, the 1:2 turn ratio transformer is used to obtain sufficiently low load impedance and thereby improving the maximum output power [29]. Fig. 13(a) shows the *Q*-factor [21], output power, and gain depending on the size of the transformer at 1.8 and 2.4 GHz. In Fig. 13(b), the outer width of the transformer was chosen as 850  $\mu$ m, considering a transformer *Q*-factor of (10 or more) and 13 dB of gain, and an output power considering loss due to additional matching devices.

Second, capacitors are used on the primary side (drain part of the amplifier stage) and the secondary side (output part) of the transformer to adjust the 1.8- and 2.4-GHz impedances to the impedance values based on the load-pull results for the same device [30], [31]. Fig. 14 shows the impedance at each frequency load based on this consideration. The capacitances required for conversion to the impedance value based on the load-pull results are 4.1 and 1 pF for  $C_{\text{drain}}$  and  $C_{\text{out}}$ , respectively. Based on this result, the output matching network is shown in Fig. 15(a). The first step is the impedance conversion for the transformer. The second step is to convert the load impedance according to the primary capacitor of the transformer. The final step is to determine the

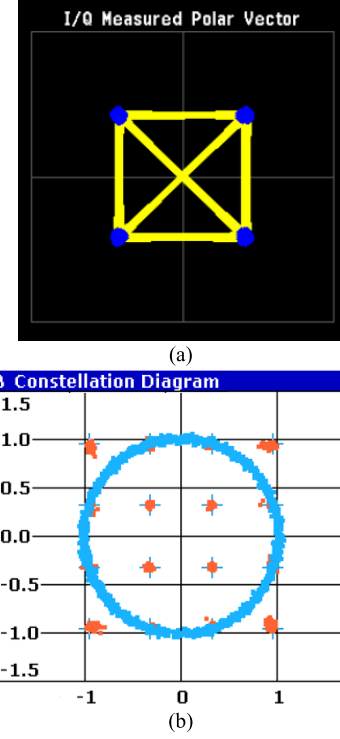


Fig. 22. Measured constellations for (a) WCDMA QPSK modulation signal ( $\text{EVM} = 3.16\%$ ) and (b) LTE 10-MHz 16-QAM modulation signal ( $\text{EVM} = 3.26\%$ ) at 0.95 GHz.

impedance position according to the secondary capacitor of the transformer for the optimum impedance position. Therefore, 1.8 and 2.4 GHz can be supported simultaneously without additional variables.

At 0.9 GHz, the gain must be reduced to 1.8 and 2.4 GHz simultaneously, with impedance conversion to the optimum point via additional tuning. The secondary side of the transformer was easy to use with additional devices. The capacitor range is 0–10 pF and the step is 1 pF. Fig. 16 shows that the optimum point can be achieved by impedance conversion using a 5-pF capacitor. At this time, the switch transistor is designed as two-stack to mitigate the breakdown problems, as shown in Fig. 16 [19]. The gate width of the transistor is 1.024 mm. When the switch is in the OFF-state, the parasitic capacitance is approximately 0.95 pF, and when it is in the ON-state for 0.9-GHz operation, the ON-resistance is 1.4  $\Omega$ . The performance degradation of the PA caused by the switch should be considered. Thus, we designed the output matching network considering the parasitic components of the switch. Fig. 17(a) shows that the harmonics are reduced using the switch on. In particular, the third harmonic was reduced by 23.2 dBc compared with the switch-off case. Fig. 17(b) indicates gain suppression at 1.8 and 2.4 GHz. In addition, the value of  $S_{22}$  is also improved. The 3-dB bandwidth is 1.46 GHz, and the fractional bandwidth is 100.7% at 1.8 and 2.4 GHz using the switch off. The 3-dB bandwidth is 0.55 GHz, and the fractional bandwidth is 58.8% at 0.9 GHz with a switch on. Fig. 17(c) shows that the loss in the 0.9-GHz band is reduced by turning the switch on.

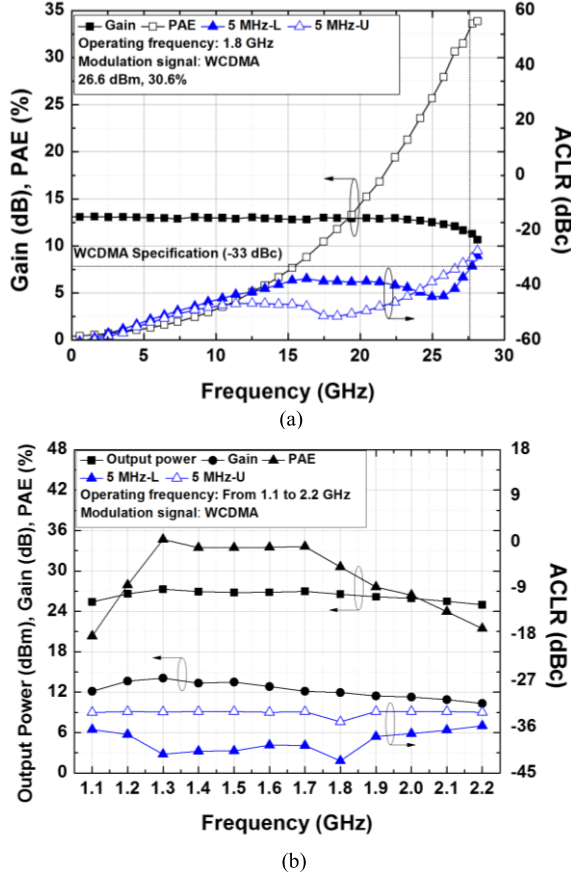


Fig. 23. Measured gain, PAE, and ACPR of the triple-band PA for WCDMA modulated signals at (a) 1.8 GHz and (b) variable frequency from 1.1 to 2.2 GHz.

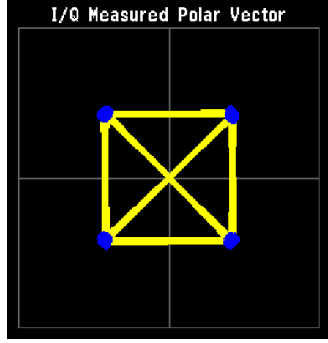


Fig. 24. Measured constellations for WCDMA QPSK modulation signal (EVM = 2.34%) at 1.8 GHz.

#### IV. IMPLEMENTATION AND MEASUREMENT RESULTS

The proposed triple-band PA was designed using the RF CMOS 180-nm 1-poly 6-metal (1P6M) process. Fig. 18 shows the overall schema. The overall size of the triple-band PA is 1.4 mm × 1.2 mm, including pads and an image of the chip showing the fabricated triple-band PA is presented in Fig. 19.

For triple-band PA, we proposed a structure that can be simultaneously supported without additional circuits in the input matching network. The total size of the input matching network is 0.8 mm × 0.37 mm, including passive devices. An additional series inductor and parallel capacitor for 50 Ω matching have values of 0.37 nH and 3 pF, respectively.

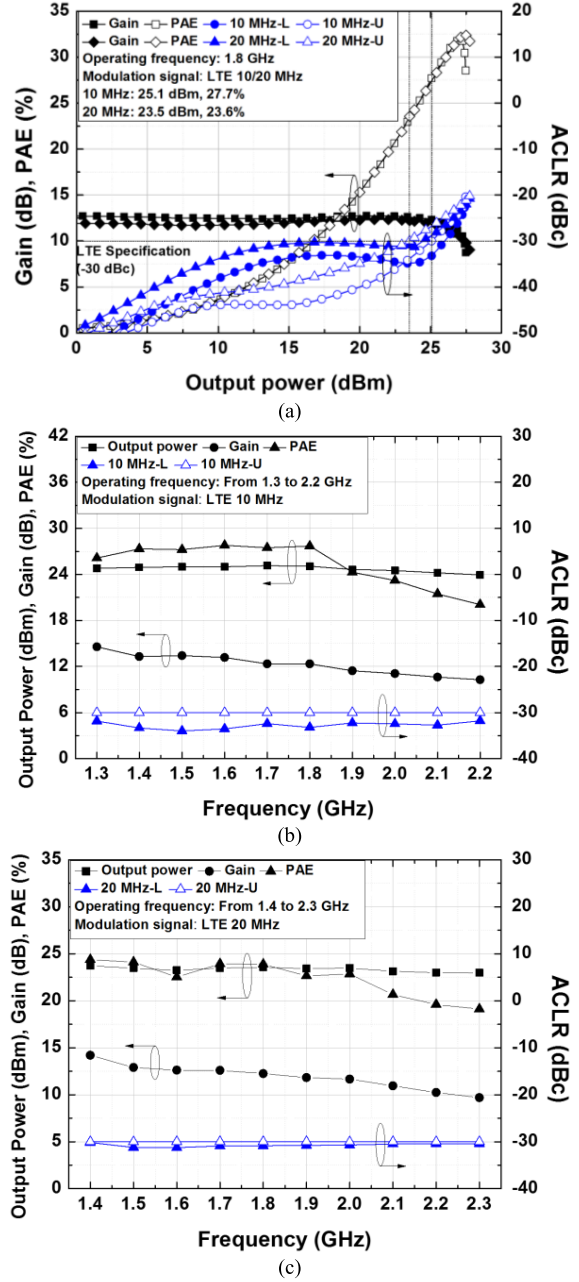


Fig. 25. Measured gain, PAE, and ACPR of the triple-band PA for (a) LTE 10/20-MHz modulated signal at 1.8 GHz, (b) LTE 10-MHz modulated signal at a variable frequency from 1.3 to 2.2 GHz, and (c) LTE 20-MHz modulated signal at a variable frequency from 1.4 to 2.3 GHz.

To support triple-band operation, we utilized the optimum transistor power-cell size obtained via the load-pull simulation and used the resistor (160 Ω) and capacitor (3.2 pF) feedback to improve the stability and linearity of the circuit [18]. The transformers for the output matching network used 1:2 turns and had a total size 0.85 mm × 0.55 mm, and an additional capacitor of 5 pF was used. These were controlled using a transistor switch.

Fig. 20 shows the S-parameters for each frequency. At 0.9 GHz, it is represented by a solid square symbol, and the performance of both  $S_{21}$  and  $S_{22}$  is improved by using an additional capacitor. The value of  $S_{11}$  is almost -9 dB in both cases.

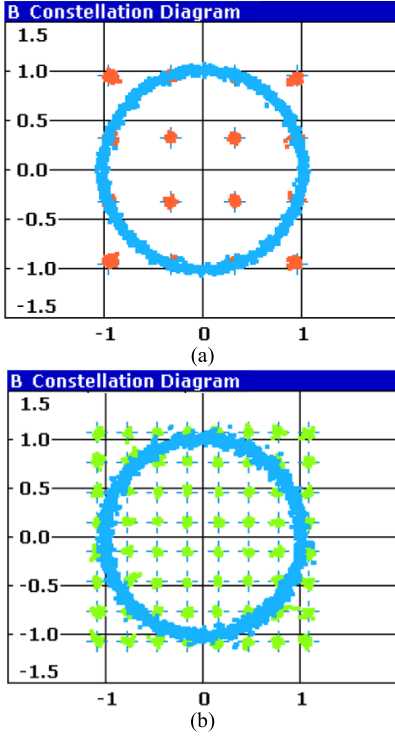


Fig. 26. Measured constellations for (a) LTE 10-MHz 16-QAM modulation signal ( $EVM = 2.83\%$ ) and (b) LTE 20 MHz 64-QAM modulation signal ( $EVM = 2.19\%$ ) at 1.8 GHz.

The fabricated triple-band PA was measured using a WCDMA modulation signal with a 3.84-MHz BW at 0.9 and 1.8 GHz, an LTE modulation signal with a 10/20-MHz BW at 0.9 and 1.8 GHz and an 802.11n WLAN modulation signal with a 20-MHz bandwidth at 2.4 GHz. The gate bias was adjusted for each modulation signal and continuous-wave (CW) signal.

#### A. 0.95 GHz: CW, WCDMA, and LTE

To characterize the gain, power, and efficiency of the PA, a CW signal was applied to the triple-band PA with the switch ON-state for the 0.95-GHz band. Fig. 21(a) shows the measured power transfer characteristics from 0.85 to 1.0 GHz. The deviations in the gain, output power, and efficiency measured within this frequency range are 0.16 dB, 1 dBm, and 1.12%, respectively. The maximum gain, output power, and efficiency of the measured results are 17 dB, 27.5 dBm, and 19% at 0.9 GHz, respectively.

Fig. 21(b) shows the gain, PAE, adjacent channel leakage ratio (ACLR), and output power of the WCDMA and LTE 10-MHz modulation signals measured at 0.95 GHz. The conditions for the WCDMA signals should be satisfied at  $-33$  dBc at a 5-MHz offset frequency, and the conditions for the LTE signals should be satisfied at  $-30$  dBc at a 10-MHz offset frequency. The average output power that satisfies the linearity of the WCDMA signal was 27.2 dBm, and the PAE was 22.9%. The average output power that satisfies the linearity of the LTE 10-MHz signal was 25.3 dBm, and the PAE

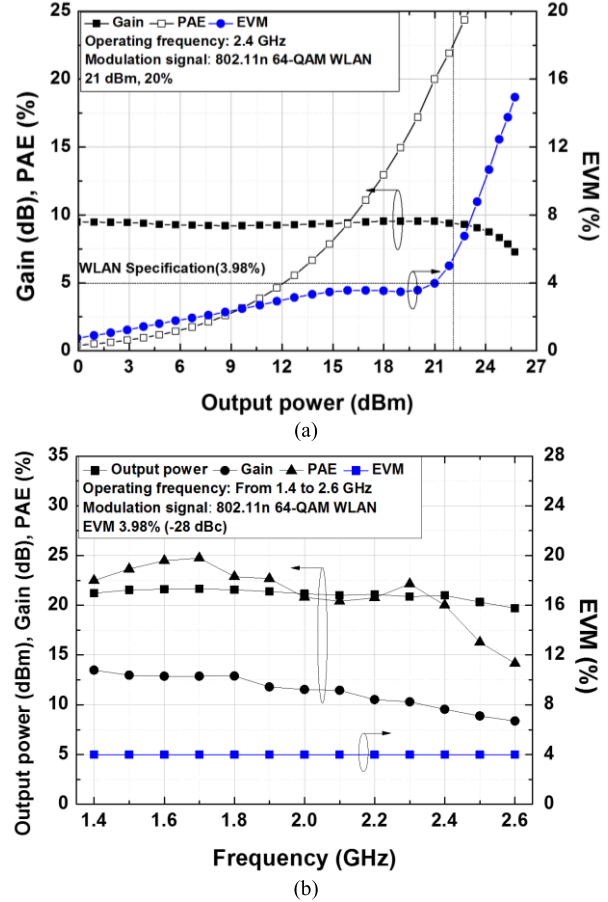


Fig. 27. Measured gain, PAE, and EVM of the triple-band PA for WLAN 802.11n modulated signal at (a) 2.4 GHz and (b) variable frequency from 1.4 to 2.6 GHz.

was 14.6%. The measured constellations for the WCDMA QPSK modulation signals and LTE 10-MHz quadratic-amplitude modulation (QAM) modulation signals are shown in Fig. 22(a) and (b), respectively.

#### B. 1.8 GHz: WCDMA and LTE

The WCDMA and LTE 10/20-MHz modulation signals were measured with a supply voltage of 3.3 V to verify the characteristics of the 1.8-GHz band. Fig. 23(a) shows the gain, PAE, ACLR, and output power of the WCDMA modulation signal in the 1.8-GHz band. The average output power that satisfies the linearity of the WCDMA signal was 26.6 dBm, and the PAE was 30.6%. The output power within the range that satisfies the linearity from 1.1 to 2.2 GHz was 25–27.3 dBm, and the PAE range was 20.3%–34.7%, as shown in Fig. 23(b). The measured constellation for the WCDMA QPSK modulation signals is shown in Fig. 24.

Fig. 25(a) shows the gain, PAE, ACLR, and output power of the LTE 10/20-MHz modulation signal in the 1.8-GHz band. The average output power that satisfies the linearity of the LTE 10-MHz signal was 25.1 dBm, and the PAE was 27.7%. In the case of the LTE 20-MHz signal, the average power was 23.5 dBm, and the PAE was 23.6%. The output

TABLE I  
COMPARISON OF STATE-OF-THE-ART CMOS MULTI-BAND PAs

Ref.	No. of Bands	Tech. (nm)	V <sub>DD</sub> (V)	Freq. (GHz)	P <sub>linear</sub> (dBm)	PAE (%)	Modulation Signal	No. of Stages	Size (mm <sup>2</sup> )	Configuration
[6]	2	CMOS 40	3.3	0.65	18.2	-	802.11n 64-QAM, 20-MHz, 2%	1	1.98 × 1.61	Single PA
				0.88	18.4	-				
[8]	Wide-band	CMOS 110	3.4, 3.5	1.8–2.3	27.3	26.1 -33	LTE 16-QAM, 10-MHz, -30 dBc	2	2.52 × 0.9	Single PA
[9]	4	CMOS 110	3.3	0.9	26.2	19.4	EDGE, -54 dBc@400 KHz WCDMA, 3.84-MHz, -33 dBc	2	3 × 3 (package)	Multiple PAs
				1.9	26.7	25.6				
				26	25					
[32]	3	BiCMOS 180	3.5	1.95	25.6	-	WCDMA, 3.84-MHz, -33 dBc	3	1 × 2.6	Single PA
				2.45	20.2	-	802.11g 64-QAM, 20-MHz, 3%			
				2.35	24.7	19	<sup>1</sup> LTE 16-QAM, 20-MHz, -33 dBc			
This Work	3	CMOS 180	3.2	0.95	27.2	22.9	WCDMA, 3.84-MHz, -33 dBc	1	1.4 × 1.2	Single PA
				25.3	14.6		LTE 16-QAM, 10-MHz, -30 dBc			
			3.3	1.8	26.6	30.6	WCDMA, 3.84-MHz, -33 dBc			
				25.1	27.7		LTE 16-QAM, 10-MHz, -30 dBc			
				23.5	23.6		LTE 64-QAM, 20-MHz, -30 dBc			
				2.4	21	20	802.11n 64-QAM, 20-MHz, 3.98%			

<sup>1</sup>standalone MMPA

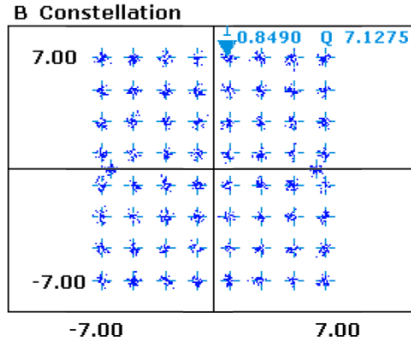


Fig. 28. Measured constellation for WLAN 802.11n 64-QAM modulation signal at 2.4 GHz.

power within the range that satisfies the linearity of the LTE 10-MHz signal from 1.3 to 2.2 GHz is 24 to 25.1 dBm, and the efficiency is 20.1% to 27.8%, as shown in Fig. 25(b). The output power within the range satisfy the linearity of the LTE 20-MHz signal from 1.4 to 2.3 GHz was 23–23.6 dBm, and the PAE was 19.1%–24.4%, as shown in Fig. 25(c). The measured constellations for LTE 10-MHz 16-QAM modulation signals and LTE 20-MHz 64-QAM modulation signals are shown in Fig. 26(a) and (b), respectively.

#### C. 2.4 GHz: WLAN 802.11n

The WLAN 802.11n 64-QAM modulation signals were measured for a supply voltage of 3.3 V to verify the characteristics of the 2.4-GHz band. Fig. 27(a) shows the measurement results for the WLAN in the 2.4-GHz band. The average output power that satisfies the linearity of an error vector magnitude (EVM) of 3.98% was 21 dBm, and the PAE was 20%. Fig. 27(b) shows the results according to the frequency sweep. The frequency was 1.4–2.6 GHz, the output power was 19.7–21.6 dBm, and the PAE was 14.2%–24.7%. The measured constellation for the WLAN 802.11n 64-QAM modulation signals is shown in Fig. 28.

The measured performance of the triple-band PA is summarized and compared with the performance of various multi-band PAs in Table I.

#### V. DISCUSSION

Although a single-stage design was used to verify its structure, the proposed PA is easy to implement with a multistage design. For example, in the case of a two-stage PA, the input and output matching networks can be implemented via the method proposed in this article, and the interstage can be designed in the same way as the input matching network.

Moreover, because the transistors used in the driver stage are smaller than those used in the power stage, the loading effect is reduced in the driver stage. Therefore, it is expected that the multistage PA can easily have multiband characteristics, in contrast to the single-stage PA. Furthermore, when designing a two-stage PA, additional linearization techniques, such as antiphase can be used to suppress the nonlinearity of the power stage through the driver stage. Thus, the linearity of the PA can be improved [33]–[35].

#### VI. CONCLUSION

In this article, we proposed a triple-band PA using an input variable matching network structure and minimal output passive elements. The designed triple-band PA was fabricated using a 180-nm CMOS process. The CW, WCDMA, and LTE 10-MHz signals were used in the 0.95-GHz band. The output powers were 28.1, 27.2, and 25.3 dBm, respectively, and the PAEs were 18.4%, 22.9%, and 14.6%, respectively. The WCDMA and LTE 10/20-MHz signals were used in the 1.8-GHz band, and the output powers and efficiencies were 26.6, 25.1, and 23.5 dBm and 30.6%, 27.7%, and 23.6%, respectively. Finally, the WLAN signal was used in the 2.4-GHz band, and the output power and efficiency were 21 dBm and 20%, respectively. These results verify that the proposed design can use a single chip to satisfy triple-band wireless mobile applications.

## REFERENCES

- [1] P. A. Dal Fabbro and M. Kayal, *Linear CMOS RF Power Amplifier for Wireless Applications*. Berlin, Germany: Springer, 2010.
- [2] I. Aoki *et al.*, "A fully-integrated quad-band GSM/GPRS CMOS power amplifier," *IEEE J. Solid-State Circuits*, vol. 43, no. 12, pp. 2747–2758, Dec. 2008.
- [3] Y. Cho, D. Kang, J. Kim, D. Kim, B. Park, and B. Kim, "A dual power-mode multi-band power amplifier with envelope tracking for handset applications," *IEEE Trans. Microw. Theory Techn.*, vol. 61, no. 4, pp. 1608–1619, Apr. 2013.
- [4] P. Colantonio, F. Giannini, R. Giofrè, and L. Piazzon, "A design technique for concurrent dual-band harmonic tuned power amplifier," *IEEE Trans. Microw. Theory Techn.*, vol. 56, no. 11, pp. 2545–2555, Nov. 2008.
- [5] F. G. S. Silva, R. N. de Lima, R. C. S. Freire, and C. Plett, "A switchless multiband impedance matching technique based on multiresonant circuits," *IEEE Trans. Circuits Syst. II, Exp. Briefs*, vol. 60, no. 7, pp. 417–421, Jul. 2013.
- [6] B. Kim, D.-H. Lee, S. Hong, and M. Park, "A multi-band CMOS power amplifier using reconfigurable adaptive power cell technique," *IEEE Microw. Wireless Compon. Lett.*, vol. 26, no. 8, pp. 616–618, Aug. 2016.
- [7] C. Presti, F. Carrara, A. Scuderi, P. Asbeck, and G. Palmisano, "A 25 dBm digitally modulated CMOS power amplifier for WCDMA/EDGE/OFDM with adaptive digital predistortion and efficient power control," *IEEE J. Solid-State Circuits*, vol. 44, no. 7, pp. 1883–1896, Jul. 2009.
- [8] K. Kim, J. Ko, S. Lee, and S. Nam, "A two-stage broadband fully integrated CMOS linear power amplifier for LTE applications," *IEEE Trans. Circuits Syst., II, Exp. Briefs*, vol. 63, no. 6, pp. 533–537, Jun. 2016.
- [9] J. Park, C. Lee, and C. Park, "A quad-band CMOS linear power amplifier for EDGE applications using an anti-phase method to enhance its linearity," *IEEE Trans. Circuits Syst. I, Reg. Papers*, vol. 64, no. 4, pp. 765–776, Apr. 2017.
- [10] W. Kim, K. S. Yang, J. Han, J. J. Chang, and C. H. Lee, "An EDGE/GSM quad-band CMOS power amplifier," *IEEE J. Solid-State Circuits*, vol. 49, no. 10, pp. 2141–2149, Oct. 2014.
- [11] S. Kang, U. Kim, and J. Kim, "A multi-mode multi-band reconfigurable power amplifier for 2G/3G/4G handset applications," *IEEE Microw. Wireless Compon. Lett.*, vol. 25, no. 1, pp. 49–51, Jan. 2015.
- [12] U. Kim, S. Kang, J. Woo, Y. Kwon, and J. Kim, "A multiband reconfigurable power amplifier for UMTS handset applications," *IEEE Trans. Microw. Theory Techn.*, vol. 60, no. 8, pp. 2532–2542, Aug. 2012.
- [13] N.-C. Kuo *et al.*, "A 0.4-to-4-GHz all-digital RF transmitter package with a band-selecting interposer combining three wideband CMOS transmitters," *IEEE Trans. Microw. Theory Techn.*, vol. 66, no. 11, pp. 4967–4984, Nov. 2018.
- [14] K. Kim, D.-H. Lee, and S. Hong, "A dual-mode multi-band second harmonic controlled SOI LDMOS power amplifier," *IEEE Microw. Wireless Compon. Lett.*, vol. 25, no. 7, pp. 466–468, Jul. 2015.
- [15] S. Hu, S. Kousai, and H. Wang, "A broadband mixed-signal CMOS power amplifier with a hybrid class-G Doherty efficiency enhancement technique," *IEEE J. Solid-State Circuits*, vol. 51, no. 3, pp. 598–613, Mar. 2016.
- [16] J. Ko and S. Nam, "A two-stage S-/X-band CMOS power amplifier for high-resolution radar transceivers," *IEEE Microw. Wireless Compon. Lett.*, vol. 28, no. 7, pp. 606–608, Jul. 2018.
- [17] J. S. Park, S. Hu, Y. Wang, and H. Wang, "A highly linear dual-band mixed-mode polar power amplifier in CMOS with an ultra-compact output network," *IEEE J. Solid-State Circuits*, vol. 51, no. 8, pp. 1756–1770, Aug. 2016.
- [18] S. Jin, B. Park, K. Moon, M. Kwon, and B. Kim, "Linearization of CMOS cascode power amplifiers through adaptive bias control," *IEEE Trans. Microw. Theory Techn.*, vol. 61, no. 12, pp. 4534–4543, Dec. 2013.
- [19] F. Carrara, C. D. Presti, F. Pappalardo, and G. Palmisano, "A 2.4-GHz 24-dBm SOI CMOS power amplifier with fully integrated reconfigurable output matching network," *IEEE Trans. Microw. Theory Techn.*, vol. 57, no. 9, pp. 2122–2130, Sep. 2009.
- [20] H. Wang, C. Sideris, and A. Hajimiri, "A CMOS broadband power amplifier with a transformer-based high-order output matching network," *IEEE J. Solid-State Circuits*, vol. 45, no. 12, pp. 2709–2722, Dec. 2010.
- [21] W. Ye, K. Ma, and K. S. Yeo, "2.5 A 2-to-6 GHz class-AB power amplifier with 28.4% PAE in 65 nm CMOS supporting 256 QAM," in *IEEE ISSCC Dig. Tech. Papers*, Feb. 2015, pp. 1–3. doi: 10.1109/ISSCC.2015.7062914.
- [22] I. Aoki, S. Kee, D. Rutledge, and A. Hajimiri, "Distributed active transformer—a new power-combining and impedance-transformation technique," *IEEE Trans. Microw. Theory Techn.*, vol. 50, no. 1, pp. 316–331, Jan. 2002.
- [23] O. El-Gharniti, E. Kerherve, and J.-B. Begueret, "Modeling and characterization of on-chip transformers for silicon RFIC," *IEEE Trans. Microw. Theory Techn.*, vol. 55, no. 4, pp. 607–615, Apr. 2007.
- [24] D. M. Pozar, *Microwave Engineering*, 4th ed. Hoboken, NJ, USA: Wiley, 2011, pp. 559–562.
- [25] K. H. An *et al.*, "Power-combining transformer techniques for fully-integrated CMOS power amplifiers," *IEEE J. Solid-State Circuits*, vol. 43, no. 5, pp. 1064–1075, May 2008.
- [26] B.-H. Ku, S.-H. Baek, and S. Hong, "A wideband transformer-coupled CMOS power amplifier for X-band multifunction chips," *IEEE Trans. Microw. Theory Techn.*, vol. 59, no. 6, pp. 1599–1609, Jun. 2011.
- [27] T. Oka *et al.*, "A high-power low-distortion GaAs HBT power amplifier for mobile terminals used in broadband wireless applications," *IEEE J. Solid-State Circuits*, vol. 42, no. 10, pp. 2123–2127, Oct. 2007.
- [28] G. Nikandish, E. Babakrur, and A. Medi, "A harmonic termination technique for single- and multi-band high-efficiency class-F MMIC power amplifiers," *IEEE Trans. Microw. Theory Techn.*, vol. 62, no. 5, pp. 1212–1220, May 2014.
- [29] C. Park, J. Han, H. Kim, and S. Hong, "A 1.8-GHz CMOS power amplifier using a dual-primary transformer with improved efficiency in the low power region," *IEEE Trans. Microw. Theory Techn.*, vol. 56, no. 4, pp. 782–792, Apr. 2008.
- [30] Q. Cai, W. Che, K. Ma, and L. Gu, "A concurrent dual-band high-efficiency power amplifier with a novel harmonic control network," *IEEE Microw. Wireless Compon. Lett.*, vol. 28, no. 10, pp. 918–920, Oct. 2018.
- [31] Y. Lee and S. Hong, "A dual-power-mode output matching network for digitally modulated CMOS power amplifier," *IEEE Trans. Microw. Theory Techn.*, vol. 61, no. 4, pp. 1570–1579, Apr. 2013.
- [32] M. L. Lee, C. Y. Liou, W. T. Tsai, C. Y. Lou, H. L. Hsu, and S. G. Mao, "Fully monolithic BiCMOS reconfigurable power amplifier for multi-mode and multi-band applications," *IEEE Trans. Microw. Theory Techn.*, vol. 63, no. 2, pp. 614–624, Feb. 2015.
- [33] S. Kang, D. Baek, and S. Hong, "A 5-GHz WLAN RF CMOS power amplifier with a parallel-cascaded configuration and an active feedback linearizer," *IEEE Trans. Microw. Theory Techn.*, vol. 65, no. 9, pp. 3230–3244, Sep. 2017.
- [34] J. Park, C. Lee, J. Yoo, and C. Park, "A CMOS antiphase power amplifier with an MGTR technique for mobile applications," *IEEE Trans. Microw. Theory Techn.*, vol. 65, no. 11, pp. 4645–4656, Nov. 2017.
- [35] C. Lu, A. V. H. Pham, M. Shaw, and C. Saint, "Linearization of CMOS broadband power amplifiers through combined multigated transistors and capacitance compensation," *IEEE Trans. Microw. Theory Techn.*, vol. 55, no. 11, pp. 2320–2328, Nov. 2007.



**Milim Lee** (S'13) received the B.S. and M.S. degrees in electronic engineering from Soongsil University, Seoul, South Korea, in 2013 and 2015, respectively, where she is currently pursuing the Ph.D. degree.

Her current research interests include CMOS RF power amplifiers and transceivers for wireless chip-to-chip communication.



**Changkun Park** (S'03–M'08) received the B.S., M.S., and Ph.D. degrees in electrical engineering from the Korea Advanced Institute of Science and Technology (KAIST), Daejeon, South Korea, in 2001, 2003, and 2007, respectively.

From 2007 to 2009, he was with the Advanced Design Team of the DRAM Development Division, Hynix Semiconductor Inc., Icheon, South Korea, where he was involved in the development of high-speed I/O interfaces of DRAM. In September 2009, he joined the Faculty of the School of Electronic Engineering, Soongsil University, Seoul, South Korea. His current research interests include RF and millimeter-wave circuits, RF CMOS power amplifiers, and wireless chip-to-chip communication and power transfers.